Remarkable rigidity of the single α-helical domain of myosin-VI revealed by NMR spectroscopy

C. Ashley Barnes,[a] Yang Shen,[a] Jinfa Ying,[a] Yasuharu Takagi,[b] Dennis A. Torchia,[a] James R. Sellers[b] and Ad Bax[a,*]

[a] Laboratory of Chemical Physics, NIDDK,

[b] Laboratory of Molecular Physiology, NHLBI

National Institutes of Health, Bethesda, MD, 20892-0520, USA

SUPPORTING INFORMATION

Hydrodynamic modeling

Assuming a protein density of 1.4 g/cm^3, and a mass of 7.96 kD for the center 60 residues of the MT domain, we modeled this section of the domain as a cylinder with a volume of 10,000 Å^3. With an unhydrated length of 60 × 1.5 Å, this yields a radius of 6 Å prior to making the "bare atom correction" of 2 Å,[1] effectively accounting for the presence of protein hydrogen atoms at the molecular surface, and an additional 1-Å correction to account for the hydration layer.[1] Adding these corrections then results in a model cylinder of length l_{cyl} = 96 Å and a radius r_{cyl} = 9 Å. Rotational diffusion of an axially symmetric rotor such as cylinder is characterized by two diffusion constants $D_{//}$ and $D_{\perp}$, describing rotation about the long (symmetry) and short axes of the cylinder, respectively. The correlation functions needed to calculate R_1, R_2 and the NOE depend upon (a) the angle made by the internuclear N-H vector and the long axis of the helix, 14°, for an ideal α–helix, and (b) three correlation times τ_A, τ_B and τ_C given by $\tau_A = 1/6D_{\perp}$; $\tau_B = 1/(D_{//}+5D_{\perp})$; $\tau_C = 1/(4D_{//}+2D_{\perp})$. Since $l_{cyl} >> r_{cyl}$, $D_{//} >> D_{\perp}$ and hence $\tau_A > \tau_B > \tau_C$. Herein we employ expressions of Garcia de la Torre and Bloomfield[2-3] which yield $D_{//} / D_{\perp} = 7.6$ and $\tau_m = 1/(2D_{//}+4D_{\perp}) = 10.3$ ns.

^{1}H-^{1}H NOE simulations

The signal intensities of NOESY cross-peaks of protons *i* and *j* are proportional to proton-proton cross-relaxation rates, σ_{ij}. The σ_{ij} are functions of (a) the overall correlation times of the helix, (b) the internuclear H_i-H_j distance (2.8 Å for H_i-$H_{i\pm1}$), and (c) the angle made by the H_i-H_j internuclear vectors and the long axis of the helix. In addition, an order parameter $\boldsymbol{S}_{HH}^2$ that accounts for internal motion of the H_i-H_j internuclear vector scales σ_{ij}. The NOESY spectrum was recorded using a large mixing time (0.25 s) in order to ensure adequate signal-to-noise of the cross-peak intensities. Spin-diffusion effects were accounted for in the calculations by including cross-relaxation involving seven spins in the simulations of the cross-peak intensities (Figure S6A). The calculations also accounted for the fact that each amide site was 8% deuterated. Rate matrices and populations were calculated for the fully protonated state and the six states in which a single deuteron was present. The small population of remaining states (ca. 8%) containing more than one deuteron, was divided by six and added to the population of each of the six single-deuteron states. The values of $I_{i\pm1}/I_d$ so calculated are about 10% smaller than those calculated assuming 100% protonation. Cross-relaxation rates are calculated for an idealized a-helix with an axially symmetric diffusion tensor, with its unique axis parallel to the helix axis, an interproton H^N—H^N distance of 2.8 Å,[4] τ_m = 10.3 ns and ρ = 7.6. For a mixing time of 0.25, the calculation yields a value of $I_{i\pm1}/I_d = 0.33$, somewhat larger than the average measured value of $I_{i\pm1}/I_d$, ca. 0.28, for residues near the center of the helix. (Figure S6B). The observation that the calculated value of $I_{i\pm1}/I_d$ exceeds the measured value, is in part due to the implicit assumption in the calculation that $\boldsymbol{S}_{HH}^2 = 1$. Indeed, the observed decrease in $I_{i\pm1}/I_d$ as residue positions recede from the center of the helix, following the behavior of ^{15}N R_2 (Figure 6C, main text).

Structure calculations

Structural models for SAH were obtained using the XPLOR-NIH software package[5] via a standard Cartesian molecular dynamics simulated annealing refinement protocol, starting from the coordinates of an idealized α-helical structure with backbone torsion angles of $\phi = -62.5°$, $\psi = -42.5°$, $\omega = 180°$. The protocol included 400,000 steps of 2 fs each, with the temperature linearly ramped down from 3000 to 25 K, followed by a Powell energy minimization. Fitted experimental restraints included the newly measured $^1D_{NH}$, $^1D_{C'N}$, $^2D_{C'H}$ RDCs from the Pf1 medium (with 100 mM NaCl) and $^1D_{HN}$ RDCs measured in Pf1 with no NaCl, scaled by the inverse or the ^{15}N R_2 to account for differential dynamics (see main text). Empirical force fields included quadratic bond, angle, and improper terms with force constants of 5000 kcal**.**Å^{-2}**.**mol, 500 kcal**.**rad^{-2}**.**mol^{-1} and 500 kcal**.**rad^{-2}**.**mol, respectively, as well as a quartic repulsive-only non-bonded potential with a force constant of 4 kcal**.**Å^{-2}**.**mol^{-1}. In addition, backbone/backbone hydrogen bonding geometries were restrained via a potential of mean force (HBDB term in XPLOR-NIH).[6] Fixed magnitude alignment tensors were used during the structural calculations, with the axial and rhombic components of each alignment tensor determined by SVD fitting of the R_2-scaled RDCs, of each alignment condition, to an idealized α-helix. Force constants for different types of RDCs in two different alignment media were obtained from a combination of force constants (0.4 kcal**.**Hz^{-2}**.**mol^{-1} for $^1D_{NH}$; 0.1 kcal**.**Hz^{-2}**.**mol^{-1} for $^1D'_{C'N}$; 0.2 kcal**.**Hz^{-2}**.**mol^{-1} for $^2D'_{C'H}$, where $^1D'_{C'N} = 8.27\times{}^1D_{C'N}$ and $^2D'_{C'H} = 3.10\times{}^2D_{C'H}$, with $^1D'_{C'N}$ and $^2D'_{C'H}$ being the values normalized[7] to the $^1D_{NH}$ couplings) that yielded best cross validation performance according to a grid searching procedure. The $^1D_{NH}$ RDC force constant multipliers (and thereby the multipliers for the other types of RDCs) were ramped up with a constant multiplicative factor throughout the protocol from 0.05 to 2.5; i.e., at 25 K, the $^1D_{NH}$ force constant was ramped up to 1 kcal**.**Hz^{-2}**.**mol^{-1}.

The ten lowest energy structures obtained from the above refinement protocol were then used as starting conformers for modeling the side-chain conformations in implicit solvent using empirical energy terms of the XPLOR-NIH software. In addition to the energy terms used in the above backbone refinement protocol, two empirical terms, torsionDBPot and eefxPot, were used to model the side-chain conformations. A total of 50 structures was generated for each starting model, and the lowest energy structure was retained for each of the ten starting conformers and then deposited in the PDB (entry 6OBI).

RDCs *versus* persistence length

We derive the scaling of the averaged second order Legendre polynomial for a worm-like chain, $\langle P_2(\cos(\beta_n))\rangle$, as a function of position n from the origin (tagging site), fully analogous to the derivation by Landau and Lifshitz[8] of $\langle\cos(\beta_n)\rangle = \exp(-n/L_P)$. Following Landau and Lifshitz, the angles between the tangents, t_a, t_b, and t_c at three points a, b, and c on the chain are related by

$$\cos\theta_{ac} = \cos\theta_{ab}\cos\theta_{bc} - \sin\theta_{ab}\sin\theta_{bc}\cos\phi_{ab,bc} \qquad \text{(A1)}$$

where $\phi_{ab,bc}$ is the angle between the planes (t_a, t_b) and (t_b, t_c). Bearing in mind that in a worm-like chain the fluctuations of curvature for sections ab and bc for a given direction of t_b are statistically independent, i.e., $\langle\cos\phi_{ab,bc}\rangle = 0$, averaging over a large distribution of worm like chains, all co-aligned at the origin, yields

$$< \cos \theta_{ac} > = < \cos \theta_{ab} > < \cos \theta_{bc} > \quad \text{(A2)}$$

Eq. A2 shows that the mean value of q_n at position n is a multiplicative function of the number of intervening segments, n, relative to the origin of the chain, i.e., must be an exponentially decreasing function $\exp(-n/L_P)$, with L_P being the persistence length.

Below, we first show that analogous to eq A2, $< P_2(\cos \theta_{ac}) > = < P_2(\cos \theta_{ab}) > < P_2(\cos \theta_{bc}) >$, i.e., that $< P_2(\cos \theta_n) >$ also is an exponentially decaying function:

$$< P_2(\cos \theta_{ac}) > = < 3(\cos^2 \theta_{ab} \cos^2 \theta_{bc} + \sin^2 \theta_{ab} \sin^2 \theta_{bc} / 2) - 1 > / 2 \quad \text{(A3)}$$

where we again used $< \cos \phi_{ab,bc} > = 0$ and $< \cos^2 \phi_{ab,bc} > = ½$. Eq. A3 can be rewritten as

$$< P_2(\cos \theta_{ac}) > = < 3 \cos^2 \theta_{ab} \cos^2 \theta_{bc} + {}^3/_2 (1 + \cos^2 \theta_{ab} \cos^2 \theta_{bc} - \cos^2 \theta_{ab} - \cos^2 \theta_{bc}) - 1 > / 2$$

$$= < 9 \cos^2 \theta_{ab} \cos^2 \theta_{bc} + 3 (1 - \cos^2 \theta_{ab} - \cos^2 \theta_{bc}) > /4$$

$$= < 3(\cos^2 \theta_{ab} - 1) / 2 > < 3(\cos^2 \theta_{bc} - 1) / 2 >$$

$$= < P_2(\cos \theta_{ab}) > < P_2(\cos \theta_{bc}) > \quad \text{(A4)}$$

For small values of θ, $\cos \theta \approx 1 - \theta^2/2$, and $P_2(\cos \theta) \approx 1 - 3\theta^2/2$; i.e. $< P_2(\cos \theta_n) >$ decays three times faster than $< \cos \theta_n >$, or:

$$< P_2(\cos \theta_n) > = \exp (-3n / L_P) \quad \text{(A5)}$$

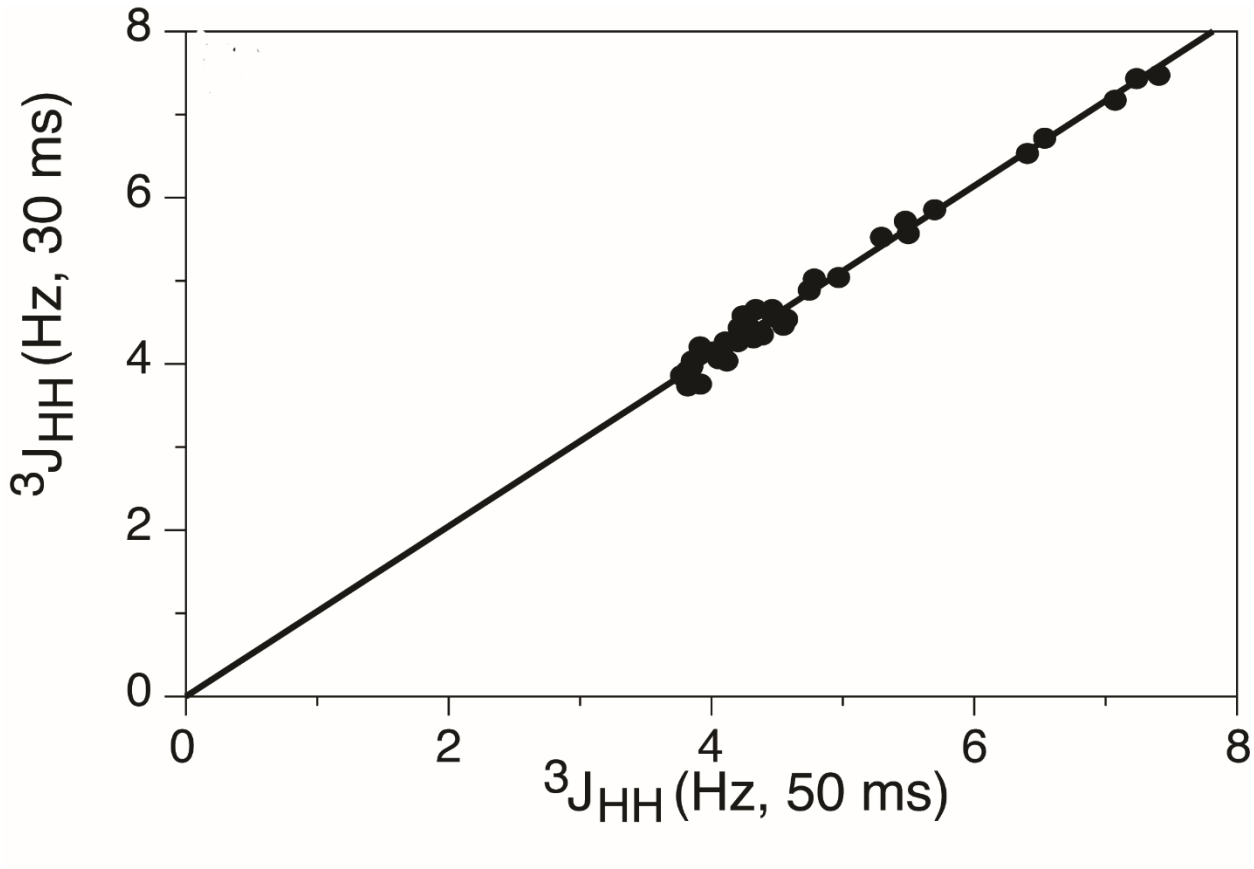

Figure S1. Correlation plot between the $^3J_{HNH\alpha}$ values measured with dephasing durations of 30 and 50 ms. Data were collected at 900 MHz using the ARTSY-J experiment,[9] on fully protonated, ^{15}N-enriched 1 mM MT at pH 6.3, 35 °C and are uncorrected for $^1H^{\alpha}$ spin flips.

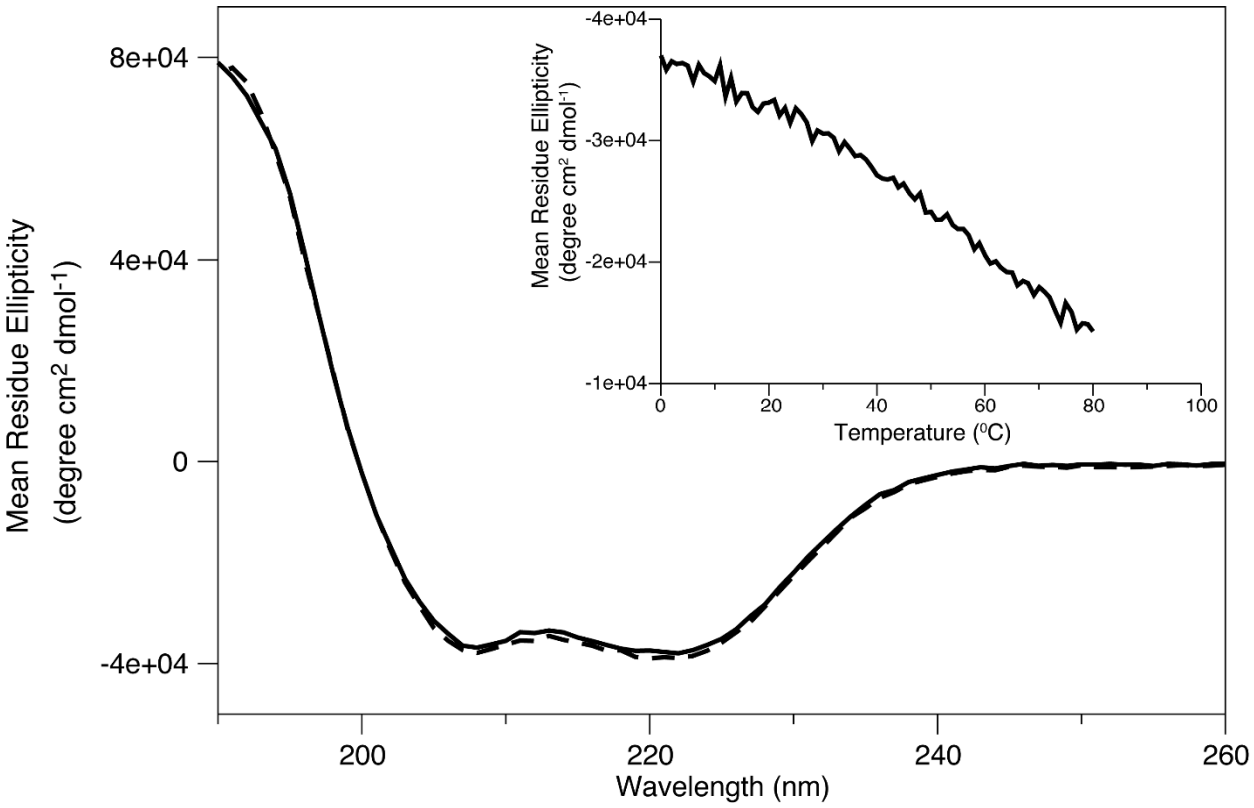

Figure S2. Circular dichroism spectra of the E68W MT domain (10 μM) in 20 mM sodium phosphate, 2 mM EDTA, pH=6.3 at 0 °C before (solid) and after (dashed) thermal melt measurements (inset), which report the mean residue ellipticity at 222 nm from 0°C to 80°C. The helicity of the MT at 0 °C is 97% as calculated by the CDNN program.[10]

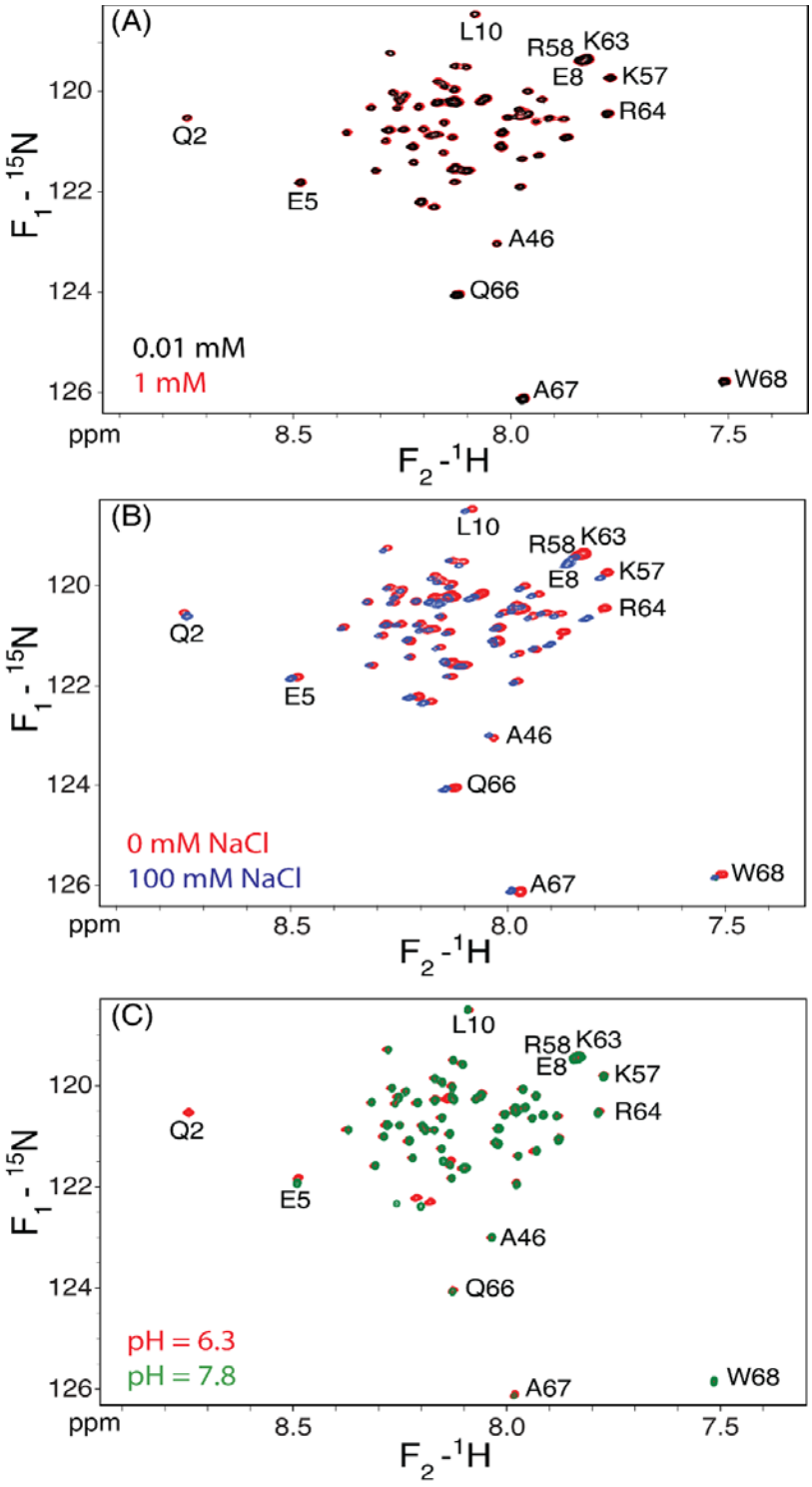

Figure S3. Comparison of 900 MHz TROSY-HSQC spectra of perdeuterated ^{15}N-labeled E68W MT recorded under different conditions. (A) Spectra recorded in 20 mM sodium phosphate, 2 mM EDTA, pH=6.3 at 20 °C and concentrations of 10 µM (black) and 1 mM (red). (B) Spectra recorded in 20 mM sodium phosphate, 2 mM EDTA, pH=6.3 at 20 °C in the absence (red) and presence (blue) of 100 mM NaCl. (C) Spectra in 20 mM sodium phosphate, 2 mM EDTA, at 20 °C in the absence of 100 mM NaCl, at pH 6.3 (red) and 7.8 (green).

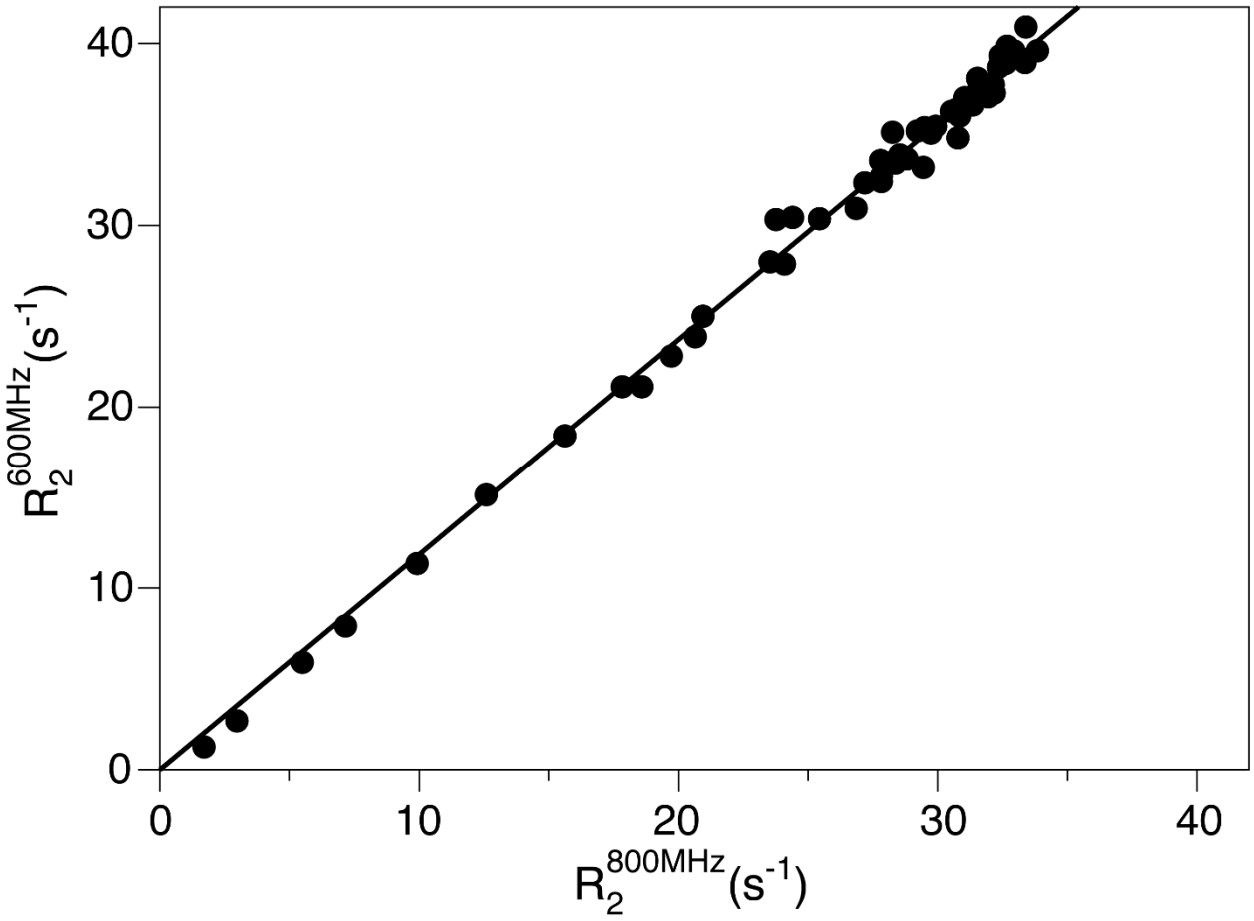

Figure S4. Correlation plot of ^{15}N $R_{1\rho}$ values measured at 14.1 (600 MHz) and 18.8 T (800 MHz ^{1}H frequency), using a 2.5 kHz spin lock field. On-resonance $R_{1\rho}$ values are derived from the measured values using the small, standard adjustment for off-resonance effects: $R_{1\rho} = (R_{1\rho}' - \sin^2\phi\, R_1) / \cos^2\phi$, where $R_{1\rho}'$ is the experimentally measured value, and $R_{1\rho}$ is the on-resonance value.

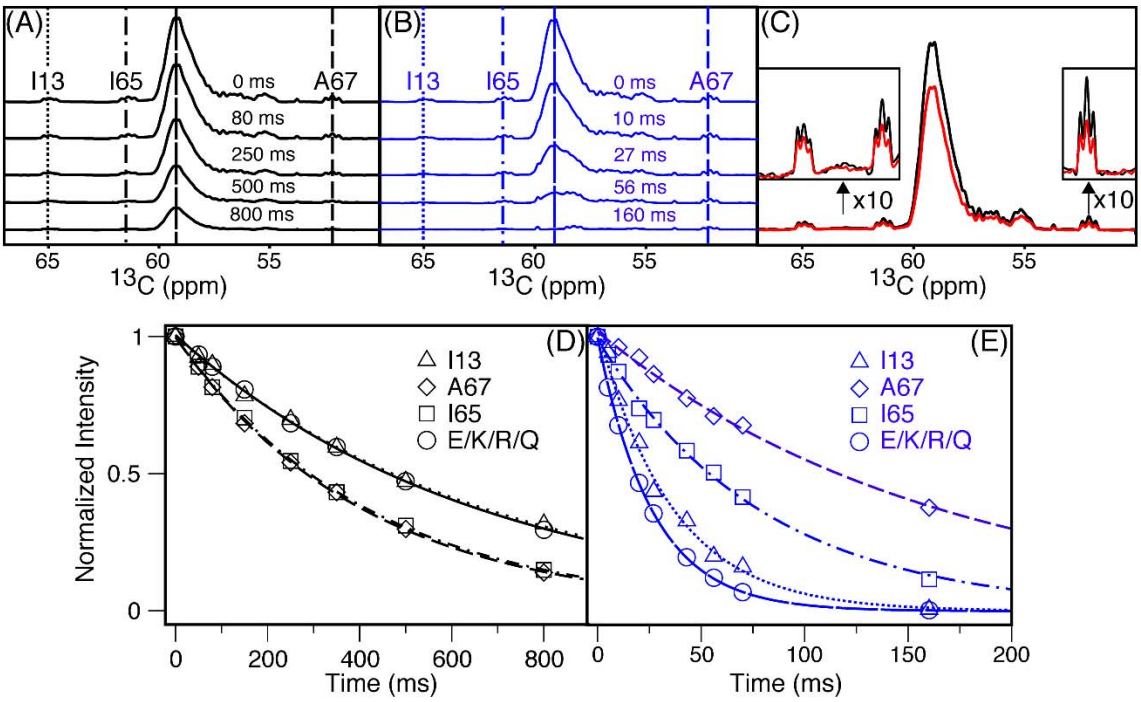

Figure S5. Direct observe $^{13}C^{\alpha}$ relaxation measurements of uniformly $^{15}N/^{13}C$-enriched E68W MT at 14 T, 20 °C. (A) R_1 measurements were carried out with the Freeman-Hill modification[11] of the regular inversion-recovery experiment, such as to allow for a two-parameter fit. Specifically, we fit the difference in signal between a 180°-T-90°-Observe and a 90°-Observe experiment as a function of T. The 180° pulse is of the hyperbolic secant type[12] centered at 100 ppm. Results of the fits are listed in Table S5. (B) $R_{1\rho}$ measurement, using a 2.5 kHz spin lock field with the carrier placed at 56 ppm. (C) Heteronuclear ^{13}C-{^1H} NOE measurement. The spectra result from 1024 transients with (black) and without (red) ^1H saturation during the 3 s delay between scans. The insets show the isolated signals of I13, I65 and A67 at 10 times higher scale. (D, E) Decay curves, taken at the positions indicated in (A, B).

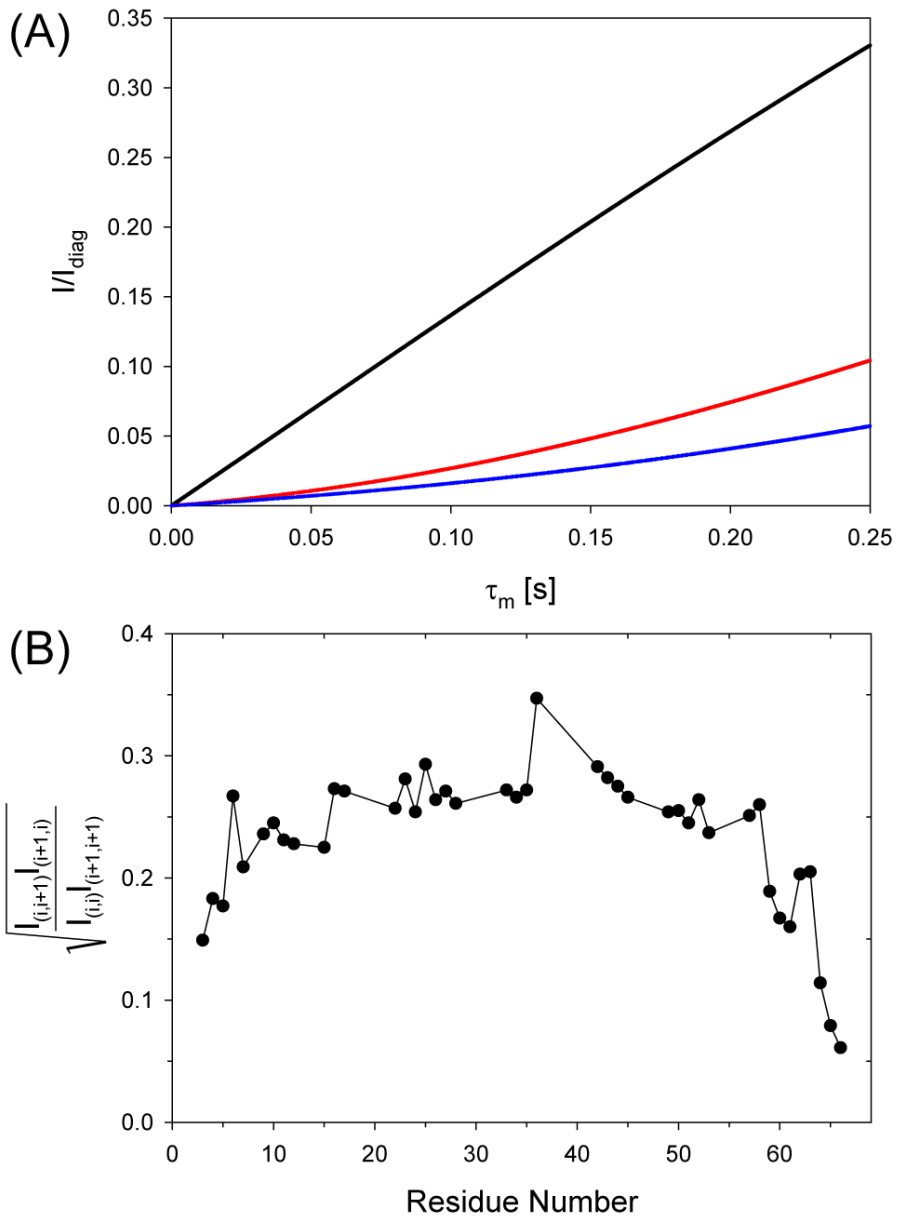

Figure S6. ^{1}H-^{1}H NOE intensities in the MT domain. (A) Calculated NOE intensities as a function of mixing time in an ideal α-helix. Intensities are calculated for a system of seven sequential amide protons, using the spectral densities for an axially symmetric diffusion tensor with $D_{//} / D_{\perp} = 7.6$ and $\tau_m = 10.3$ ns (SI Text). The solid black line corresponds to the intensity of the $d_{NN}(4,4\pm1)$ cross peaks divided by the intensity of the spin 4 diagonal peak. Colored lines (red and blue) correspond to the respective intensities of the $d_{NN}(4,4\pm2)$ and $d_{NN}(4,4\pm3)$ cross peaks divided by the intensity of the spin-4 diagonal. (B) Normalized intensity of sequential H^N-H^N NOE cross peaks observed in the 250 ms mixing time 4D NOESY spectrum of MT, recorded at 900 MHz ^{1}H frequency, 20 °C. Values are only shown for well-resolved peaks whose intensities could be accurately measured.

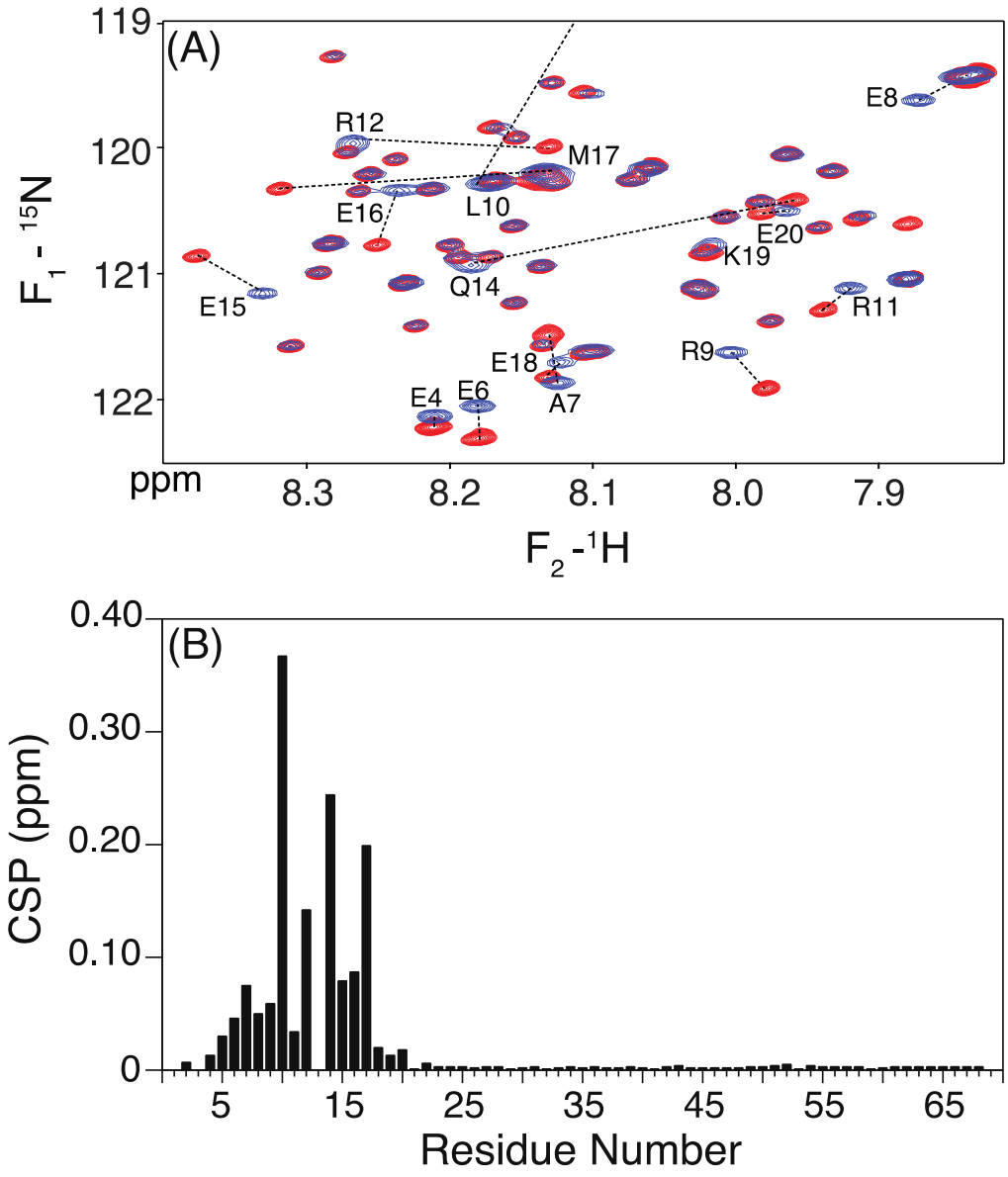

Figure S7. Chemical shift perturbation of E68W MT domain upon I13C mutation. (A) Overlay of the most crowded region of the E68W (red) and E68W/I13C (blue) ^{1}H-^{15}N TROSY-HSQC spectra of MT, recorded at 900 MHz, 20 °C, 2 mM EDTA, pH 6.3. Dashed lines connect resonance that are perturbed most; peak labels correspond to E68W/I13C MT (B) The chemical shift perturbation, calculated as CSP = $\sqrt{(\Delta\delta^{15}\mathrm{N}/5)^2 + (\Delta\delta^{1}\mathrm{H})^2}$, where Δδ denotes the chemical shift difference in units of ppm.

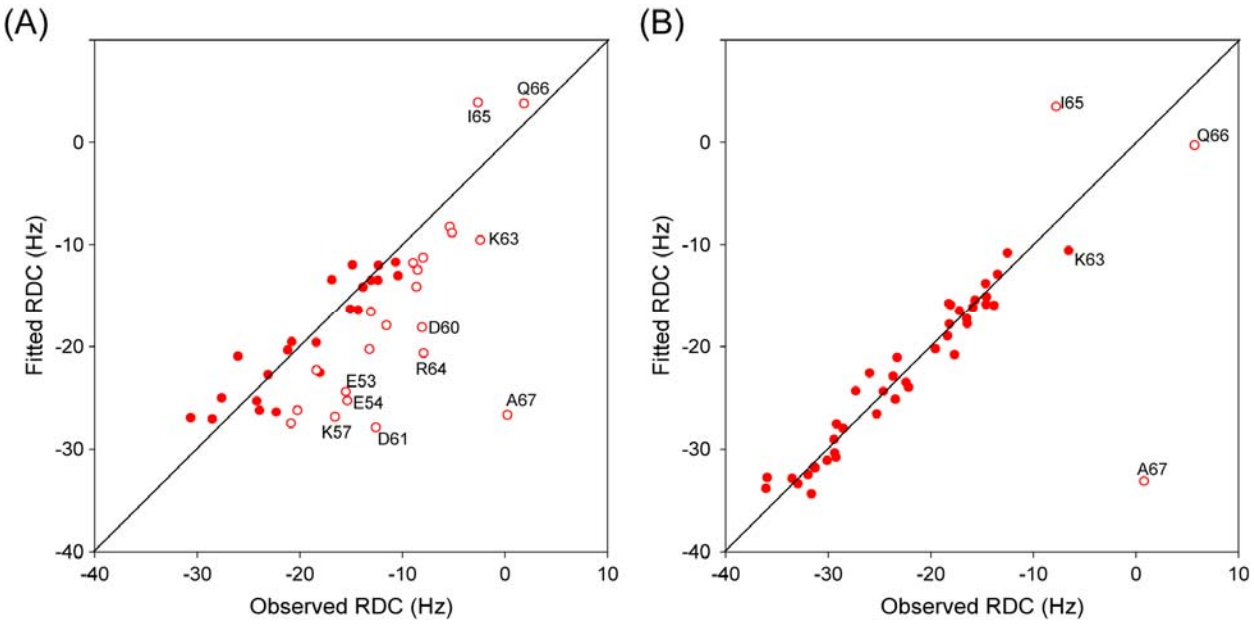

Figure S8. Plot of SVD best-fitted RDC data of DOTA-M8-Tm tagged I13C mutant of E68W MT in 20 mM sodium phosphate, 2 mM EDTA, 100 mM NaCl, 900 MHz, 20 °C. (A) Alignment tensor best fit to the $^1D_{NH}$ of residues R24-E45. (B) Alignment tensor best fit to the $^1D_{NH}$ of residues R24-R64, after upscaling of $^1D_{NH}$ by *exp*[(+(*i*-13)/49.75]. Open symbols in each panel correspond to residues not included in the SVD fit.

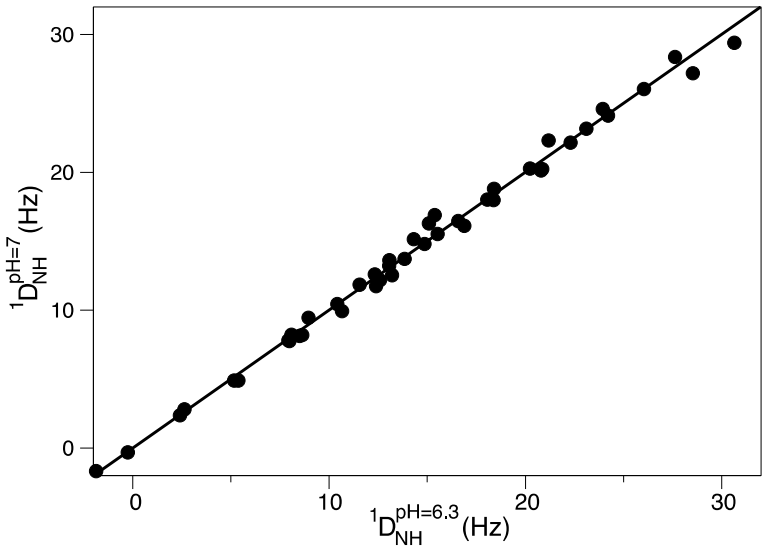

Figure S9. Correlation plot of the RDC data of DOTA-M8-Tm tagged I13C mutant of E68W MT in 20 mM sodium phosphate, 2 mM EDTA, 100 mM NaCl, 900 MHz, 20 °C at pH 6.3 versus pH 7.0. The pairwise RMSD between the two sets of values is 0.3 Hz**.**

Table S1. Chemical shifts and $^{3}J_{HNH\alpha}$ values of the native MT domain as well as chemical shifts of the I13C/E68W double mutant, recorded in 20 mM sodium phosphate, 2 mM EDTA, pH=6.3. ^{1}H and ^{15}N chemical shifts are at 20 °C; $^{13}C^{\alpha}$ and $^{13}C^{\beta}$ shifts are at 35 °C.

Residue	^{1}H (ppm)	^{15}N (ppm)	^{1}H (ppm)[a]	^{15}N (ppm)[a]	$^{13}C^{\alpha}$ (ppm)	$^{13}C^{\beta}$ (ppm)	$^{3}J_{HNH\alpha}$ (Hz)
Q2	8.79	120.01	8.80	119.99			
Q3	8.18	119.71	8.19	119.69			
E4	8.26	121.70	8.25	121.63	57.56	27.81	6.1
E5	8.54	121.30	8.52	121.18	57.80	28.93	5.1
E6	8.23	121.78	8.23	121.55	58.53	28.75	4.9
A7	8.18	121.00	8.17	121.37	54.71	17.31	4.2
E8	7.89	118.95	7.92	119.15	58.21	28.45	
R9	8.03	121.40	8.05	121.14	59.24	29.36	4.1
L10	8.14	118.02	8.22	119.80	57.28	40.47	4.2
R11	7.99	120.78	7.97	120.64	58.87	28.99	4.3
R12	8.18	119.49	8.32	119.46	58.89	28.93	4.4
I13 (C13)	7.93	120.12	(8.22)	(118.24)	64.46	37.36	4.4
Q14	8.01	119.92	8.23	120.44	58.55	27.26	4.3
E15	8.43	120.35	8.38	120.66	59.04	28.78	4.1
E16	8.30	120.27	8.29	119.84	58.83	28.52	
M17	8.37	119.82	8.17	119.67	58.45	31.75	4.2
E18	8.18	121.31	8.17	121.22	58.45	28.52	4.2
K19	8.07	120.34	8.07	120.28	59.27	31.50	
E20	8.03	120.00	8.02	120.01	58.44	28.44	
R21	8.16	121.13	8.16	121.13	59.23	28.86	
K22	8.16	119.07	8.15	119.08	58.77	31.26	4.4
R23	7.96	120.06	7.96	120.05	58.72	29.04	4.4
R24	8.22	119.34	8.22	119.35	58.86	29.11	4.5
E25	8.25	120.27	8.25	120.28	58.86	28.84	4.6
E26	8.34	120.49	8.34	120.50	58.89	28.63	4.4
D27	8.36	121.07	8.36	121.09	57.07	40.41	3.9
K28	8.24	120.37	8.25	120.39	58.85	28.48	4.3
Q29	8.18	118.99	8.18	119.00	58.47	27.35	4.6
R30	8.15	121.12	8.15	121.12			
R31	8.18	119.71	8.18	119.70	59.06	29.06	
R32	8.20	119.43	8.20	119.43	58.86	29.12	4.3
K33	8.03	120.87	8.03	120.88	58.75	31.18	3.9
E34	8.29	119.59	8.29	119.60	58.92	28.63	4.2
E35	8.22	120.36	8.22	120.37	58.79	28.52	4.5

E36	8.19	121.06	8.19	121.07	58.81	28.67	4.3
E37	8.31	119.84	8.31	119.86	59.05	28.65	3.9
R38	8.07	120.34	8.07	120.34	59.13	29.05	
R39	8.17	119.78	8.18	119.80			
M40	8.33	118.77	8.33	118.78			
K41	8.07	120.65	8.07	120.65			
L42	7.99	120.13	7.99	120.14	57.54	40.71	4.3
E43	8.27	120.90	8.27	120.92	58.83	28.71	4.7
M44	8.32	119.53	8.32	119.54	59.14	31.45	4.8
E45	8.21	120.73	8.21	120.74	58.56	28.60	
A46	8.09	122.50	8.09	122.50	54.44	17.18	4.0
K47	8.03	119.93	8.03	119.94	58.46	31.40	4.7
R48	8.06	120.05	8.06	120.06	58.49	28.99	4.2
K49	8.12	119.76	8.12	119.76	58.61	31.39	4.4
Q50	7.98	119.68	7.98	119.69	58.68	28.68	4.5
E51	8.31	119.70	8.31	119.72	58.68	28.62	4.5
E52	8.19	120.43	8.19	120.45	58.55	28.73	4.8
E53	8.21	120.13	8.21	120.13	58.59	28.71	4.6
E54	8.26	119.83	8.26	119.84	58.42	28.67	4.7
R55	8.07	120.59	8.08	120.62			
K56	8.01	119.58	8.01	119.56	58.13	31.52	5.2
K57	7.83	119.30	7.83	119.30	57.98	31.57	5.9
R58	7.89	118.95	7.88	118.91			
E59	8.22	119.78	8.22	119.78	57.70	29.04	5.7
D60	8.35	120.28	8.34	120.27	55.49	40.27	5.3
D61	8.28	120.62	8.28	120.59	55.54	40.27	5.6
E62	8.10	119.64	8.11	119.66	57.32	29.05	5.8
K63	7.90	119.18	7.89	118.94	56.46	31.55	6.4
R64	7.89	120.44	7.83	120.01	56.33	29.64	6.8
I65	8.02	120.95	7.93	120.54	61.05	37.59	7.7
Q66	8.28	123.61	8.18	123.56	55.31	28.68	7.4
A67	8.23	125.85	8.03	125.63	52.04	18.68	7.0
E68 (W68)	7.95	125.34	(7.57)	(125.34)	57.54	30.36	7.7

[a]I13C E68W MT

Table S2. Backbone RDCs and isotropic *J* values (Hz) of the W68 MT domain in 20 mM sodium phosphate, 2 mM EDTA, 100 mM NaCl, pH=6.3 measured in the absence and presence of 13 mg/mL Pf1 at 20 °C. Experimental uncertainties in the measured couplings are 0.5 Hz ($^1D_{NH}$), 0.2 Hz ($^1D_{NC'}$) 0.4 Hz ($^2D_{C'H}$), 0.3 Hz ($^1J_{NH}$), 0.1 Hz ($^1J_{NC'}$) and 0.2 Hz ($^2J_{C'H}$). Couplings are listed according to the residue number of the amide ^1H or ^{15}N and ignore the negative sign of the ^{15}N gyromagnetic ratio.

Res	$^1D_{NH}$	$^1D_{NH}$[a]	$^1D_{NC'}$	$^2D_{C'H}$	$^1J_{NH}$	$^2J_{C'H}$	$^1J_{NC'}$
Q2	-7.3	2.2	0.4	-0.2	92.9	3.8	14.9
E4	-11.4	-2.1	-0.6	-4.2	93.0	4.2	15.3
E5	-9.9	1.0	1.5	1.0	93.3	4.1	15.1
E6	-19.3	-6.6	0.9	-1.1	92.9	4.3	15.1
A7	-25.2	-13.8	0.9	-2.8	92.9	4.4	14.6
R9	-22.1	-7.9	1.5	-0.5	93.2	4.3	14.8
L10	-24.9	-13.5	1.4	-1.5	93.3	4.4	14.9
R11	-25.6	-11.4	0.4	-3.7	93.1	4.4	15.2
R12	-21.9	-6.1			93.5		
I13	-23.7	-10.8	1.3	-1.3	93.0	4.0	15.3
Q14	-28.5	-15.4	1.6	-2.5	92.7	4.3	14.9
E15	-26.0	-8.8	0.6	-2.7	92.5	4.1	14.9
E16	-22.2	-6.5	2.1	0.3	93.1	4.2	15.1
M17	-27.0	-13.7	1.1	-1.4	93.4	4.2	15.0
E18	-30.5	-16.1	1.2	-4.1	93.5	4.0	15.2
K22	-30.5	-13.6	0.8	-3.5	93.7	4.2	15.1
R23	-27.3	-8.8	2.0	-0.1	93.0	4.3	15.0
R24	-28.5	-15.0	1.1	-2.5	93.9	4.2	15.0
E25	-33.7	-18.9	0.9	-4.2	92.9	4.2	15.0
E26	-29.4	-10.2			92.8		
D27	-28.7	-12.0	2.2	0.1	93.4	4.4	15.2
K28	-31.9	-18.6	1.0	-3.8	93.7	4.1	15.1
Q29	-32.0	-17.9	1.0	-4.2	93.4	4.1	14.9
R32	-28.3	-20.6	1.5	-3.9	93.2	4.1	14.9
K33	-32.6	-14.7	0.9	-3.9	92.7	4.3	15.1
E34	-32.4	-12.1			92.7		
E35	-30.8	-17.7	1.0	-1.8	93.0	4.3	15.1
E37	-31.3	-13.6			91.9		
R39	-31.6		0.6	-2.0	92.6	4.4	14.9
M40	-29.9	-17.5			93.2	4.3	14.9
L42	-27.5	-18.0	1.3	-2.9	92.9	4.4	15.1
E43	-32.0	-20.3	1.4	-3.3	93.3	4.3	15.2
M44	-28.9	-12.1			93.1		
E45	-30.6	-11.9	2.4	0.7	93.4	4.4	15.1
A46	-34.6	-18.7	1.2	-2.9	92.9	4.2	15.1
R48	-30.0	-11.0	1.3	0.0	92.9	4.2	15.2
K49	-33.7	-14.1			93.0		

Q50	-34.1	-20.4	1.3	-2.9	92.5	4.3	15.0
E51	-28.5	-15.7			93.6		
E52	-30.4	-9.3	2.3	0.2	92.9	4.3	15.2
E53	-33.5	-17.3	1.2	-0.9	93.3	4.2	14.9
E54	-29.7	-19.1	1.4	-3.4	93.0	4.3	15.2
K56	-25.5	-10.6	2.3	0.9	92.9	4.3	15.0
K57	-29.9	-17.8	1.0	-2.6	93.1	4.3	15.0
E59	-31.8	-6.4	1.5	0.0	93.1	4.3	15.1
D60	-25.5	-11.6	1.2	-0.2	93.3	4.2	15.3
D61	-25.1	-14.8	1.1	-2.2	93.3	4.1	15.2
E62	-28.7	-7.1	0.6	-1.6	93.0	4.0	15.2
R64	-19.5	-8.4	0.7	-0.5	93.1	4.1	15.4
I65	-21.3	-2.5	0.3	-0.1	93.1	4.2	15.3
Q66	-22.9	2.7	0.3	0.9	92.9	4.1	14.9
A67	-16.8	1.1	0.3	1.4	92.6	4.0	15.1

[a] measurements in the absence of 100 mM NaCl

Table S3. Experimental validation statistics for different structural representations of MT.[a]

	Ideal α-helix	Exp. structure
Q_{free} (%)[b]	21.1/27.4/13.9/17.7 (32.0) [b]	-
Q_{free} (%)[c]	15.6/16.5/13.9/15.9 (27.1) [c]	12.9/13.8/12.5/12.0 (22.8) [c,d]
Q_{fit} (%)[e]	-	10.4/7.1/12.2/11.9 (15.9) [e]

[a] For residues E6-K63.

[b] reported Q factors are for all/$^{1}D_{NH}$/$^{1}D_{NC'}$/$^{2}D_{C'H}$ values, respectively, measured in the sample containing 100 mM NaCl, with D_a = 15.62 Hz and R = 0.16 used for calculating the denominator of the Q factor and all couplings normalized to the 21,585 Hz ^{15}N-^{1}H dipolar interaction strength, i.e., $^{1}D_{NC'}$ and $^{2}D_{C'H}$ upscaled by 8.26 and 3.10, respectively from their experimental values. The Q factor for the $^{1}D_{NH}$ values measured from the sample without the addition of 100 mM NaCl are given in parenthesis.

[c] same as b but the Q factors are reported for all/$^{1}D_{NH}$/$^{1}D_{NC'}$/$^{2}D_{C'H}$ values, respectively, after upscaling by the inverse of the ^{15}N R_2 rate (see main text), and with a D_a = 16.88 Hz and R = 0.16.

[d] Free Q factors for the RDC-refined structure (see main text).

[e] Q factors reported for the ensemble of lowest energy final RDC-refined structures, for which all couplings of residues E6 to K63 were used.

Table S4. ^{15}N relaxation rates of the MT domain in 20 mM sodium phosphate, 2 mM EDTA, pH=6.3, 20 °C, measured at 600 and 800 MHz ^{1}H frequency, and best fit dynamics parameters obtained using Modelfree4 while restraining the diffusion tensor to be axially symmetric with τ_m = 10.3 ns, and ρ = 7.5. TROSY R_2 values ($R_{2,TR}$) correspond to ^{15}N Hahn-echo decay rates. All R_1 and R_2 rates are in units of s^{-1}, and errors are estimated at ±3%

	R_1 [a]	R_1 [b]	R_2 [a]	R_2 [b]	NOE [b]	τ_e (ps)	S^2
Q2							
E4							
E5							
E6	0.86	1.10	27.9	24.1	0.35	1000	0.71
R9	0.79	0.99	30.9	26.9	0.39	1000	0.75
L10	0.77	0.99	30.4	24.4	0.42	980	0.77
R11	0.76	0.96	32.4	27.8	0.42	1100	0.76
R12	0.76	0.94	32.7	27.8	0.47	1100	0.78
I13	0.73	0.93	32.3	27.2	0.46	1000	0.79
Q14	0.70	0.90	33.7	28.8	0.50	1100	0.81
E15	0.69	0.88	35.1	29.7	0.48	1100	0.80
E16	0.70	0.90	33.2	29.4	0.49	1100	0.81
M17	0.67	0.87	35.2	29.2	0.51	1100	0.82
E18	0.68	0.86	34.8	30.8	0.50	1100	0.82
E20	0.61	0.82	36.3	30.5	0.54	1000	0.86
K22	0.58	0.78	37.0	31.0	0.55	1000	0.87
R23	0.58	0.77	38.1	31.5	0.54	1000	0.87
R24	0.59	0.76	36.6	31.3	0.57	1000	0.88
E25							
E26							
D27	0.54	0.73	39.0	33.4	0.52	920	0.88
E28	0.52	0.71	39.2	32.7	0.59	900	0.91
Q29	0.52	0.69	37.8	32.1	0.56	760	0.91
R32	0.52	0.70	39.3	32.4	0.56	820	0.91
K33							
E34	0.50	0.67	39.6	33.8	0.54	810	0.91
E35	0.51	0.71	39.1	32.7	0.58	830	0.91
E37	0.49	0.67	40.9	33.4	0.56	810	0.91
M40	0.50	0.68	38.9	32.6	0.53	710	0.91
L42	0.53	0.71	39.9	32.7	0.51	840	0.89
E43	0.56	0.72	37.7	32.1	0.51	870	0.88
M44	0.55	0.74	37.5	31.6	0.52	870	0.88
E45	0.57	0.76	37.1	31.9	0.50	890	0.87
A46	0.58	0.77	39.6	32.9	0.49	1000	0.85
K47	0.60	0.80	36.0	30.8	0.54	1000	0.86
R48	0.62	0.81	36.4	30.7	0.50	970	0.85
K49	0.65	0.85	35.1	28.3	0.48	930	0.84
Q50	0.65	0.86	35.4	29.9	0.49	1000	0.83
E51	0.66	0.85	35.4	29.5	0.48	1000	0.82
E52	0.69	0.89	33.4	28.4	0.47	1000	0.81

E53	0.70	0.89	33.9	28.5	0.46	1000	0.80
E45	0.71	0.90	33.6	27.8	0.43	1000	0.79
K56	0.80	1.00	30.4	25.4	0.40	1000	0.76
K57	0.82	1.02	28.0	23.5	0.36	930	0.75
E59	0.93	1.15	25.0	20.9	0.33	980	0.69
D60	0.97	1.17	22.8	19.7	0.29	940	0.66
D61	1.01	1.21	21.1	18.6	0.24	910	0.64
E62	1.08	1.28	18.4	15.6	0.23	900	0.62
K63	1.15	1.36	15.1	12.6	0.18	850	0.58
R64							
I65							
Q66							
A67							
E68							

[a] Measured at 600 MHz ^{1}H frequency
[b] Measured at 800 MHz ^{1}H frequency

Table S5. Longitudinal (T_1) and transverse ($T_{1\rho}$) $^{13}C^{\alpha}$ relaxation of the E68W MT at 600 MHz in 20 mM sodium phosphate, 2 mM EDTA, pH = 6.3 and 20 °C. MT $^{13}C^{\alpha}$ T_1 values were measured using the Freeman-Hill inversion-recovery experiment using a non-selective, hyperbolic secant ^{13}C inversion pulse. Uncertainties in the relaxation times are *ca* 3%.

Residue	T_1 (ms)[a]	$T_{1\rho}$ (ms)
E/K/R/Q	698	26
I13	713	35
I65	438	79
A67	415	160

Table S6. Hydrogen exchange rates (s^{-1}) of the E68W MT domain in 20 mM sodium phosphate, 2 mM EDTA, 7% D_2O, pH 7.8 at 20 °C and 30 °C and pH 8.9 at 20 °C

Res	20 °C pH 7.8	30 °C pH 7.8	20 °C pH 8.9
E4	17		
E5	7.5	20	
E6	6.7	20	
A7	3.0	10	
E8		6.7	
R9	0.96	3.9	17
L10	0.59	2.0	6.6
R11	0.60	2.6	8.5
R12	0.75	4.0	14
I13	0.49		5.6
Q14	0.59		10
E15	0.57	2.5	9.6
E16	0.53		7.9
M17	0.55	2.2	8.4
R18	0.78	3.5	16
E20	0.67		10
K22	0.84	3.9	14
R23	0.84		12
R24	1.1	4.0	20
E25	1.0	4.8	19
E26	0.85	3.4	13
D27	1.0	4.4	16
E28	0.82	3.3	13
Q29	0.77	2.9	12
R31	0.74	2.4	10
R32	0.77	3.5	11
K33	0.86	4.2	16
E34	0.63	2.6	9.4
E35	0.49	1.8	6.6
E36	0.36	1.1	3.3
E37	0.34	1.1	3.4
R39	0.56	2.3	7.4
M40	0.72	3.3	13
K41		3.9	
L42	0.72	2.8	9.8
E43	0.90	3.7	14
M44	1.1	5.4	21
E45	1.2	5.2	21
A46	1.3	6.2	17
K47	1.4	6.5	20

R48	1.4	6.8	19
K49	2.0	10	35
Q50	2.3	12	
E51	1.4	6.4	17
E52	1.0	4.3	15
E53	0.86	3.4	12
E54	1.0	4.3	15
R55		7.2	
Q56	2.3	11	
K57	2.9	12	
R58		14	
E59	6.2	21	
D60	4.0		
D61	3.4	11	
E62	3.4	10	
K63		16	
R64	11	30	
I65	6.7	18	
Q66	20		
A67	26		
W68	0.22	0.65	3.9

Table S7. $^{1}D_{NH}$ RDCs measured at 20 °C and 35 °C, 900 MHz, for the DOTA-M8-Tm tagged I13C mutant of E68W MT in 20 mM sodium phosphate, 2 mM EDTA, pH 6.3 and 7.0. Couplings ignore the negative sign of the ^{15}N gyromagnetic ratio.

Res	$^{1}D_{NH}^{20C,pH6.3}$	$^{1}D_{NH}^{20C,pH7.0}$	$^{1}D_{NH}^{35C,pH6.3}$
R24	-26.0	-26.0	-20.9
E25	-27.6	-28.4	-21.4
E26	-14.9	-14.8	-9.4
D27	-16.9	-16.1	-11.2
K28	-30.6	-29.3	-20.4
Q29	-21.2	-22.3	-14.6
R30	-12.3	-12.6	-8.8
R31	-20.8	-20.2	-15.1
R32	-28.5	-27.2	-19.6
K33	-15.1	-16.3	-10.6
E34	-13.9	-13.7	-10.8
E35	-24.2	-24.1	-17.0
E36	-23.1	-23.2	-16.0
E37	-13.1	-13.6	-9.2
R38	-14.3	-15.2	
R39	-23.9	-24.6	-18.4
M40	-18.4	-18.8	-12.3
K41	-10.7	-9.9	-6.4
L42	-18.1	-18.0	-12.6
E43	-22.3	-22.2	-14.8
M44	-12.4	-11.8	-7.2
E45	-10.4	-10.5	-6.4
A46	-20.2	-20.3	-13.0
K47	-18.4	-18.0	-11.7
R48	-9.0	-9.5	-5.3
K49	-13.2	-12.5	-5.7
Q50	-20.9	-20.2	-12.7
E51	-13.1	-13.2	-7.6
E52	-8.0	-7.8	-6.2
E53	-15.5	-15.5	-9.0
E54	-15.4	-16.9	-9.9
R55	-8.5	-8.1	-4.1
K56	-8.6	-8.2	-3.7
K57	-16.6	-16.5	-9.4
R58	-11.6	-11.9	-2.5
E59	-5.4	-4.9	-1.9
D60	-8.1	-8.2	-3.9
D61	-12.6	-12.2	-5.1
E62	-5.2	-4.9	-1.6
K63	-2.4	-2.4	
R64	-7.9	-7.8	-3.0
I65	-2.6	-2.8	-0.6
Q66	1.9	1.7	1.4
A67	0.3	0.3	0.3
W68			-0.2

Table S8. Alignment tensor (Saupe tensor) matrix elements from SVD fitting of experimental RDCs, upscaled for the effect of dynamics (main text) to the PDB coordinates of entry 6OBI, as obtained with the DC utility of NMRPipe.

	Saupe Matrix (x10^4)					XYZ Tait-Bryan angles (°)			Da (Hz)	Rh
Pf1[a]	-15.93	-3.95	0.00	0.00	0.00	0.0	0.0	0.0	-17.19	0.16
Pf1[b]	8.43	-0.46	1.42	-1.07	3.22	13.4	4.0	42.4	-9.98	0.24
20[c]	-13.40	18.17	2.36	0.35	-8.88	29.3	2.5	82.1	-19.86	0.50
35[d]	-9.79	4.55	-0.31	-0.31	-6.51	23.2	-1.2	95.2	-13.59	0.41

All tensors are obtained with the DC program of NMRPipe for residues 6 to 63 of the first conformer of entry 6OBI;

[a] Alignment tensor obtained from a simultaneous SVD fit of all ($^1D_{NH}$, $^2D_{C'H}$, $^1D_{C'N}$) RDCs (100 mM NaCl);

[b] Alignment tensor obtained from a SVD fit of $^1D_{NH}$ RDCs (no NaCl);

[c] Alignment tensor obtained from a SVD fit of $^1D_{NH}$ RDCs collected at 900 MHz for I13C MT, aligned by the DOTA-M8-Tm tag and 20°C, after upscaling by *exp*[(+(*i*-13)/49.75];

[d] Alignment tensor obtained from a SVD fit of $^1D_{NH}$ RDCs collected at 900 MHz for I13C MT, aligned by the DOTA-M8-Tm tag and 35°C, after upscaling by *exp*[(+(*i*-13)/36.63].

References

1. Halle, B.; Davidovic, M., Biomolecular hydration: From water dynamics to hydrodynamics. *Proc. Natl. Acad. Sci. U. S. A.* **2003,** *100* (21), 12135-12140.
2. Garcia de la Torre, P.; Bloomfield, V. A., Hydrodynamic properties of complex, rigid biological macromolecules. Theory and applications. *Quart. Rev. Biophys.* **1981,** *14*, 81-139.
3. Tirado, M. M.; Garciadelatorre, J., Rotational-Dynamics of Rigid, Symmetric Top Macromolecules - Application to Circular-Cylinders. *J. Chem. Phys.* **1980,** *73* (4), 1986-1993.
4. Wüthrich, K., *NMR of Proteins and Nucleic Acids*. John Wiley & Sons: New York, 1986.
5. Schwieters, C. D.; Kuszewski, J. J.; Clore, G. M., Using Xplor-NIH for NMR molecular structure determination. *Prog. Nucl. Magn. Reson. Spectrosc.* **2006,** *48* (1), 47-62.
6. Grishaev, A.; Bax, A., An empirical backbone-backbone hydrogen-bonding potential in proteins and its applications to NMR structure refinement and validation. *J. Am. Chem. Soc.* **2004,** *126* (23), 7281-7292.
7. Ottiger, M.; Bax, A., Determination of relative N-H-N N-C ', C-alpha-C ', andC(alpha)-H-alpha effective bond lengths in a protein by NMR in a dilute liquid crystalline phase. *J. Am. Chem.Soc.* **1998,** *120* (47), 12334-12341.
8. Landau, L. D.; Lifshitz, E. M., *Statistical Physics*. Third Edition ed.; Pergamon Press: 1980; Vol. 5.

9. Roche, J.; Ying, J. F.; Shen, Y.; Torchia, D. A.; Bax, A., ARTSY-J: Convenient and precise measurement of (3)J(HNH alpha) couplings in medium-size proteins from TROSY-HSQC spectra. *J. Magn. Reson.* **2016,** *268*, 73-81.
10. Bohm, G.; Muhr, R.; Jaenicke, R., Quantitative analysis of protein far UV circular dichroism spectra by neural networks. *Protein Eng.* **1992,** *5* (3), 191-195.
11. Freeman, R.; Hill, H. D. W., Fourier transform study of NMR spin-lattice relaxation by progressive saturation. *J. Chem. Phys.* **1971,** *54* (8), 3367-3377.
12. Silver, M. S.; Joseph, R. I.; Hoult, D. I., Highly Selective Pi/2 and Pi-Pulse Generation. *J. Magn. Reson.* **1984,** *59* (2), 347-351.